

OPTIMIZATION OF ORGANIC PHOTODETECTORS USING SCAPS-1D SIMULATION: ENHANCING PERFORMANCE OF PBDB-T-2F BASED DEVICES THROUGH LAYER CONFIGURATION AND DOPING ADJUSTMENTS

 Ahmet Sait Alali^{*a},  Murat Oduncuoglu^a,  Hmoud Al-Dmour^b, Abdelaal S.A. Ahmed^c

^aDepartment of Physics, Yildiz Technical University, Istanbul, Turkey

^bMutah University, Faculty of Science, Department of Physics, 61710, Jordan

^cChemistry department, Faculty of Science, AlAzhar University, Assuit, 71524, Egypt

*Corresponding Author email: saitnuclear@gmail.com

Received October 5, 2024; revised December 12, 2024; accepted January 7, 2025

In this study, we conducted an exploration of the optimization of various parameters of a photodetector using SCAPS-1D simulation to enhance its overall performance. The photodetector structure was modified based on the structure proposed by N.I.M. Ibrahim *et al.* (AMPC, 14(04), 55–65 (2024) by changing the order of the hole transport layer (HTL) and electron transport layer (ETL). Through the optimization of layer thicknesses and doping concentrations, we significantly improved the photovoltaic parameters of our optimized structure (FTO/PFN/PBDB-T-2F/PEDOT/Ag). The optimized device exhibited V_{oc} of 1.02V, J_{sc} of 35.20 mA/cm², FF of 84.61%, and an overall efficiency of 30.40%. Additionally, the device demonstrated a high quantum efficiency (EQ) of over 99% and responsivity peaking at 0.65 A/W, covering a broad spectral region from 300 nm to 900 nm. The results indicate the critical role of meticulous optimization in developing high-performance photodetectors, providing valuable insights into the design and fabrication of devices with superior performance characteristics.

Keywords: Organic photodetector; SCAPS-1D Simulation; Performance optimization; PBDB-T-2F: BTP-4F; PEDOT: PSS; PFN: Br
PACS: 84.60. Jt 81.05. Xj 85.60. Jb 73.61. Ph 72.80. Le

1. INTRODUCTION

For the advancement of several applications in biosensing, communication networks, and health monitoring, the organic photodetectors (OPDs) must be enhanced, as the performance enhancement of OPD leads to a higher signal amplification efficiency. It has been reported that the integration of organic field-effect transistors (OFETs) with OPDs significantly boosts the signal-to-noise ratio, which is essential for accurate physiological data extraction from photoplethysmographical (PPG) waveforms [1]. Recent advancements in materials and fabrication techniques, such as using iron-phthalocyanine (FePc) with polyamide-nylon polymer coatings, have shown promising ability to enhance the photoconductivity and the responsivity by several orders of magnitude, making OPDs more effective in UV and visible regions [2]. The development of ultrathin, self-powered OPDs with efficient exciton dissociation and charge extraction processes further enhances the sensitivity and response time, which are critical for high-performance photodetection [3]. Modifying transport layers, such as using N,N'-bis-(1-naphthyl)-N,N'-diphenyl-1,1'-biphenyl-4,4'-diamine (NPB) interfacial layers with MoO₃ can improve charge selectivity and reduce dark current, thereby increasing responsivity and detectivity [4]. Through enhanced polymer-based OPDs, detection capabilities can be extended into the near-infrared (NIR) range, allowing for applications such as real-time pulse oximetry without the need for signal amplification [5]. In addition to optimizing carrier extraction and minimizing dark current, the right thickness of interfacial layers-like SnO₂ can also improve overall device performance [6]. OPDs with upgraded active layers and other parts, such as trans-impedance amplifiers, can greatly improve signal reception and lower bit error rates in visible light communication (VLC) systems [7]. For some applications, it is essential to optimize narrow wavelength selectivity while boosting responsivity and detectivity in *p-n* junction OPDs by utilizing non-fullerene acceptors (NFAs). [8]. Photomultiplication OPDs with materials like PBDB-T and FIrpic produce excellent external quantum efficiency and detectivity, ideal for high-quality imaging without preamplifiers [9]. For efficient photodetection with high detectivity and response speed, it is critical to understand the optoelectronic behavior and address recombination losses in bilayer OPDs [10]. Thus, there is an urgent need to enhance the OPD's overall performance to meet the growing demands of modern technological applications.

In organic photovoltaic systems (OPVs), both PBDB-T-2F and BTP-4F materials are frequently utilized as active layers. These active layers usually comprise a donor and an acceptor substance that aid in the production and movement of charge carriers. For example, in the setting of ternary blending solar cells, a fullerene derivative such as PC61BM is employed as the acceptor, and high-crystallinity P3HT is used as the donor to provide low recombination efficiency and good carrier transport capacity [11]. Comparably, the exciton dissociation efficiency and optical absorption range, which are essential for the overall performance of OPVs, may be increased by using PBDB-T-2F as a donor and BTP-4F as an acceptor. Furthermore, the material characteristics can be further improved by crystallizing active layers using methods like laser irradiation. This is demonstrated in thin-film transistors, where the active layer is heated and crystallized utilizing asymmetric laser profiles [12]. In other applications, such as proton-exchange membrane fuel cells (PEMFC), the active layer comprises

perfluoro sulfonate ionomers to improve ion conductivity and performance [13]. Furthermore, developments in materials science emphasize the significance of material attributes like energy conversion efficiency and biocompatibility in a variety of applications, as demonstrated by the creation of biologic piezoelectric layers on Ti substrates [14]. Improved signal-to-noise ratios through the incorporation of optical gain in interferometers highlight the importance of material advancements for improved performance in photonic devices [15]. In general, the integration of PBDB-T-2F and BTP-4F into the active layer of OPV devices is a potentially effective method for attaining enhanced efficiency and performance, drawing upon the concepts and developments noted in several associated domains [16], [17], [18].

PEDOT: PSS (poly(3,4-ethylenedioxythiophene): poly (styrene sulfonate)) is commonly utilized material as a hole transport layer (HTL) in a variety of optoelectronic devices, such as perovskite solar cells (PSCs) and organic solar cells (OSCs). This is because of its advantageous characteristics, which include outstanding wettability, appropriate conductivity, and high optical transparency, making it a great option for improving the overall performance of the device [19]. In addition, PEDOT: PSS has outstanding environmental stability, processability, and thermoelectric qualities. These can be further enhanced by doping with nanomaterials such as carbon nanotubes (CNTs) to raise the material's Seebeck coefficient and conductivity [20]. By doping graphene oxide (GO) into PEDOT: PSS, the work function of HTL significantly improved, which is critical for better hole injection and lessens luminescence quenching at the HTL/emission layer interface, thus increasing luminance and current efficiency in perovskite light-emitting diodes (PeLEDs) [21]. Additionally, PEDOT: PSS can be altered to increase its conductivity and pattern-making capabilities, which qualifies it for flexible electronics applications with high brightness and current efficiency, like flexible PeLEDs [22]. On the other hand, low sheet resistance and high transmittance have been obtained by doping PEDOT: PSS-doped with Ag nanowires (NWs), which are desirable for flexible and transparent devices [23]. Moreover, PEDOT:PSS can promote neural stem cell adhesion, proliferation, and differentiation, suggesting applications in tissue engineering and bioelectronics [24]. However, because of its capacity to increase electron mobility and decrease recombination losses, PFN: Br (poly[(9,9-bis(3'-(N,N-dimethylamino)propyl)-2,7-fluorene)-alt-2,7-(9,9-dioctylfluorene)] bromide) is frequently employed as an ETL, and thus enhancing the overall efficiency of devices [25]. By maximizing charge transport and minimizing energy losses, PEDOT: PSS as HTL and PFN: Br as ETL can work in concert to improve the overall performance of optoelectronic devices.

In this work, we investigate how to greatly improve the performance of photodetectors by optimizing their various parameters using SCAPS-1D simulation. An apparatus called a photodetector transforms light into electrical signals that are utilized in a variety of fields, including communications, imaging, and environmental monitoring. Investigations were conducted into the impacts of temperature variations on device performance as well as the optimization of the thicknesses and doping densities of PBDB-T-2F: BTP-4F, PEDOT: PSS, and PFN: Br layers. Our study builds upon the structure proposed by N. I. M. Ibrahim et al., who reported on a device configuration of ITO/PEDOT: PSS/PBDB/PBDB-T-2F: BTP-4F/PFN: Br/Ag. The power conversion efficiency (PCE) of this configuration was 4.1%, with a V_{OC} of 0.25 V, a J_{SC} of 29.14 mA/cm², and a fill factor (FF) of 56.44%. In our study, the configuration was modified to FTO/PFN: Br/PBDB/PBDB-T-2F: BTP-4F/PEDOT: PSS/Ag, reversing the order of the HTL and ETL. Through meticulous optimization of the layer thicknesses and doping concentrations, we achieved significantly improved outcomes. The optimization process involved varying the thicknesses of HTL, ETL layers, and doping densities for the PFN: Br and PEDOT: PSS layers to achieve the highest efficiency. Our optimized structure exhibited a V_{OC} of 1.02V, a J_{SC} of 35.21 mA/cm², an FF of 84.62%, and an overall efficiency of 30.40%. This study emphasizes how important careful optimization is to create high-performance photodetectors. Through our methodical examination of the impacts of temperature, doping density, and layer thickness, we offer important insights into the design and manufacturing of photodetectors with exceptional performance qualities. The results of this investigation further the field of photodetector technology by providing useful recommendations for optimizing efficiency in practical applications.

2. METHODOLOGY

2.1 Numerical simulation and device structures

The SCAPS-1D software is widely used for numerical simulations to evaluate the optical and electrical properties of various solar cell structures [26], [27]. The SCAPS-1D software utilizes fixed sources and solves three fundamental differential equations: Poisson's equation and the continuity equations for electrons and holes, all under specific boundary conditions. Through the use of self-consistent iteration methods, SCAPS-1D effectively models solar cells, producing simulated results that closely align with experimental data. This reliability makes it an invaluable tool for predicting device performance. Researchers can use SCAPS-1D to optimize various parameters, such as layer thickness, carrier concentration, and defect density, thereby enhancing solar cell efficiency and overall performance. Consequently, SCAPS-1D plays a crucial role in the design and analysis of photovoltaic devices [28], [29], [30]. Poisson's equation for a solar cell device is as follows:

$$\frac{\partial}{\partial x} \left(-\epsilon(x) \frac{\partial V}{\partial x} \right) = q [p(x) - n(x) + N_D^+(x) - N_A^-(x) + p_t(x) - n_t(x)], \quad (1)$$

And the electron, hole continuity equations are:

$$\frac{\partial n}{\partial x} = \frac{1}{q} \frac{\partial J_n}{\partial x} + G_n - R_n, \quad (2)$$

$$\frac{\partial p}{\partial x} = -\frac{1}{q} \frac{\partial J_p}{\partial x} + G_p - R_p. \quad (3)$$

Where ε is the dielectric permittivity, V is the electric potential, and q is the electronic charge. The variables $p(x)$ and $n(x)$ represent the concentrations of free holes and free electrons, respectively. $ND+x$ and $NA-x$ are the ionized donor and acceptor concentrations. The terms $pt(x)$ and $nt(x)$ denote the trap densities for holes and electrons. Additionally, $J_{n/p}$ signify the current densities, while $G_{n/p}$ represent the generation rates, and $R_{n/p}$ correspond to the recombination rates for electrons and holes.

The physical parameters for the photodetector components in the SCAPS-1D simulation are listed in **Table 1**. These parameters are FTO, PBDB-T-2F: BTP-4F, PEDOT: PSS, and PFN: Br. Thickness, band gap, electron affinity, dielectric permittivity, effective density of states, mobility, doping densities, and thermal velocities are some of these properties. FTO serves as the transparent electrode, PFN: Br is the ETL, PBDB-T-2F: BTP-4F is the active layer responsible for light absorption and charge generation, and PEDOT: PSS acts as the HTL. The values that are supplied act as a basis for both simulation and optimization.

Table 1. Physical parameters utilized for SCAPS 1D simulation

Material properties	FTO [31]	PFN: Br (ETL)[32]	PBDB-T-2F: BTP-4F (Active layer)[33]	PEDOT:PSS (HTL) [33]
Thickness (nm)	500	5	Variable	40
Band gap (eV)	3.500	2.8	1.27	1.6
Electron affinity (eV)	4.000	4	4.03	3.4
Dielectric permittivity	9.000	5	6.1	3
Conduction band effective density of states, n_c (cm ⁻³)	2.20×10^{18}	1×10^{19}	1×10^{19}	1×10^{22}
Conduction band effective density of states, n_v (cm ⁻³)	1.80×10^{19}	1×10^{19}	1×10^{19}	1×10^{22}
Electron thermal velocity, V_e (cm/s)	1.00×10^7	1.00×10^7	1.00×10^7	1.00×10^7
Hole thermal velocity, V_h (cm/s)	1.00×10^7	1.00×10^7	1.00×10^7	1.00×10^7
Electron mobility, μ_e (cm ² /Vs)	20	2.00×10^{-6}	1.70×10^{-3}	4.5×10^{-4}
Hole mobility, μ_h (cm ² /Vs)	10	1.00×10^{-4}	2.96×10^{-4}	9.9×10^{-5}
Shallow uniform donor density, n_D (cm ⁻³)	1×10^{19}	9.00×10^{-18}	7.5×10^{16}	2.00×10^{21}
Shallow uniform acceptor density, n_A (cm ⁻³)	0	0	0	0

The photodetector and energy band diagram are shown in their entirety in **Figure 1**. Several layers known as FTO, PFN:Br (ETL), PBDB-T-2F:BTP-4F (active layer), PEDOT:PSS (HTL), and Ag within the device are shown in **Figure 1a**. Light is typically allowed in through the FTO light window, electron transport is facilitated by PFN:Br, photons are absorbed and charge carriers are produced by PBDB-T-2F:BTP-4F, hole transport is promoted by PEDOT:PSS, and Ag is the back electrode. **Figure 1b** shows the energy band diagram with conduction band (E_c) and valence band (E_v) energies, indicating efficient charge separation and transport, essential for optimal device performance.

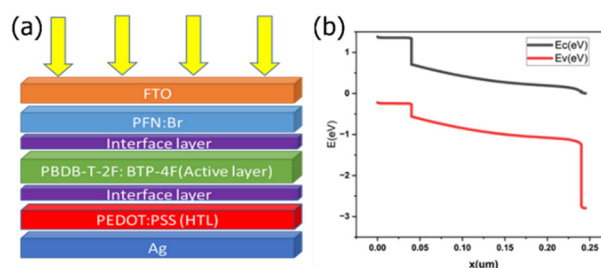


Figure 1. Schematic structure of the device, and (b) energy band diagram

3. RESULTS AND DISCUSSIONS

3.1 Optimal thickness and performance of active layer

Figure 2a depicts the effect of the thickness of the PBDB-T-2F: BTP-4F layer and performance items; open-circuit voltage (V_{OC}), current density (J_{SC}), fill factor (FF), and efficiency (η). As the layer thickness increases from 100 nm to 800 nm, V_{OC} rises steadily from 0.95V to 1.00V, and J_{SC} increases dramatically from 17 mA/cm² to roughly 35 mA/cm². FF indicates a marginal decline from 79.1% to roughly 78.5%. There was a notable increase in overall efficiency from 13.1% to around 27.5%. This shows that the ideal thickness for the PBDB-T-2F: BTP-4F layer is around 800 nm. Nonetheless, a thickness range of 700–800 nm might be chosen for practical reasons to balance production efficiency and performance.

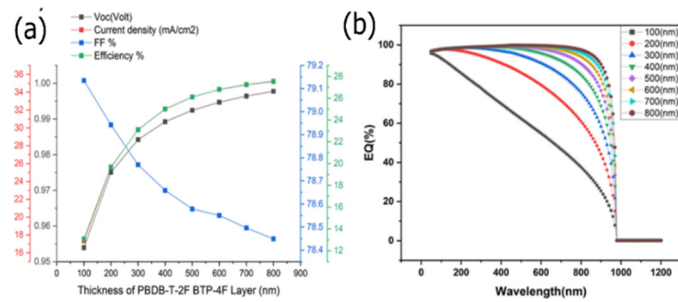


Figure 2. (a) The effect of PBDB-T-2F: BTP-4F layer thickness on photovoltaic parameters (V_{OC} , J_{SC} , FF, and η), and (b) the EQE as a function of wavelength with varying PBDB-T-2F: BTP-4F layer thickness

3.2 Impact of HTL layer thickness on device performance

Figure 3a displays the simulation-based examination of the effect of PEDOT: PSS layer thickness on several performance metrics of the device. As the thickness increases from 50 nm to 600 nm, the V_{OC} shows a tiny increase from 0.97519V to 0.977099V, suggesting a marginally beneficial impact on open-circuit voltage. With a continuous improvement, the J_{SC} goes from 25.5886 mA/cm² to 26.5829 mA/cm². The overall efficiency, which declines little from 19.6797% to 19.4037%, is negatively impacted by the FF, which falls dramatically from 78.8647% to 74.704%. The simulation-based EQE as a function of wavelength for various PEDOT: PSS layer thicknesses is shown in **Figure 3b**. The EQE curves show a comparatively constant spectrum response at different thicknesses, indicating that the device's spectral response is not significantly impacted by the thickness of the PEDOT: PSS layer.

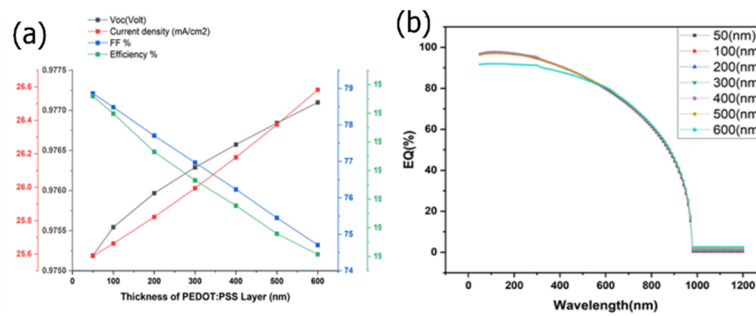


Figure 3. (a) the effect of PEDOT: PSS layer thickness on photovoltaic parameters (V_{OC} , J_{SC} , FF, and η). (b) the EQE as a function of wavelength for varying PEDOT: PSS layer thicknesses.

3.3 Impact of ETL layer thickness on device performance

The influence of different PFN: Br layer thicknesses on important performance metrics as V_{OC} , J_{SC} , FF, and η is shown by the simulation-based analysis in **Figure 4**. All the performance measures show a decrease with thickness. From **Figure 4a**, the V_{OC} of 0.975086 V, J_{SC} of 25.5741 mA/cm², FF of 78.9427%, and efficiency of 19.6859% are achieved at 5 nm. These measures show that 5 nm is the ideal thickness for the PFN: Br layer because there is a considerable decrease beyond this point. The EQE curves, displayed in panel (**Figure 4b**), further attest to the durability of the performance at the ideal thickness because they hold steady at varying thicknesses.

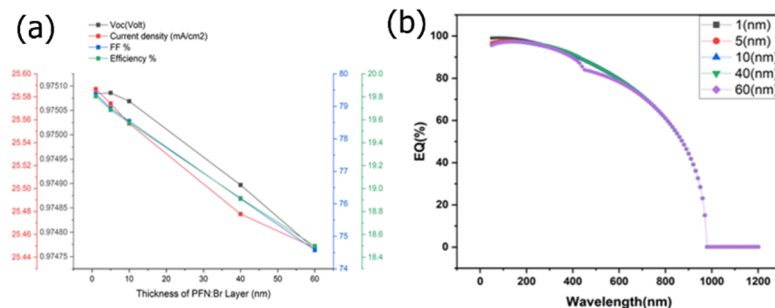


Figure 4. (a) the effect of PFN: Br layer thickness on photovoltaic parameters (V_{OC} , J_{SC} , FF, and η), and (b) the EQE as a function of wavelength for varying PFN: Br layer thicknesses

3.4 Effect of donor density of PFN: Br layer on device performance

The impact of donor density modifications in the PFN: Br layer on device performance metrics, such as V_{OC} , J_{SC} , FF, and η , is investigated in the simulation-based analysis shown in **Figure 5**. It can be observed that by increases the donor density from $10^{14}cm^{-3}$ to $10^{21}cm^{-3}$, a significant improvement in FF and η , while V_{OC} stabilizes around

10^{18}cm^{-3} as presented in **Figure 5a**. The maximum performance is observed at a donor density of 10^{21}cm^{-3} with a V_{OC} of 0.97 V, J_{SC} of 25.57 mA/cm^2 , FF of 79.53%, and an efficiency of 19.82%. Further confirming the durability of the device performance at the ideal donor density are the EQE curves displayed in panel (**Figure 5b**), which hold true for a range of donor densities.

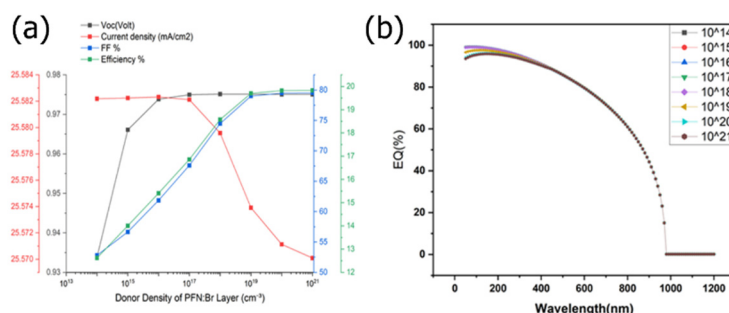


Figure 5. (a) the effect of donor density in the PFN:Br layer on photovoltaic parameters (V_{OC} , J_{SC} , FF, and η). (b) the EQE as a function of wavelength for varying donor densities in the PFN:Br layer.

3.5 Effect of acceptor density of HTL layer on device performance

The investigation performed using simulation, as illustrated in **Figure 6**, display how different acceptor densities in the PEDOT: PSS layer affect the V_{OC} , J_{SC} , FF, and η parameters. **Figure 6a**, illustrates a clear trend were increasing the acceptor density from 10^{14}cm^{-3} to 10^{21}cm^{-3} significantly enhances the FF and η . The V_{OC} also shows a steady increase, reaching 1.0058 V at the highest acceptor density. Optimal device performance is observed at an acceptor density of 10^{21}cm^{-3} with a V_{OC} of 1.0058 V, J_{SC} of 25.5714 mA/cm^2 , FF of 85.38%, and an efficiency of 21.96%. It is supported that device performance is robust at greater acceptor densities by the EQE curves shown in panel (**Figure 6b**), which are essentially consistent across a range of acceptor densities.

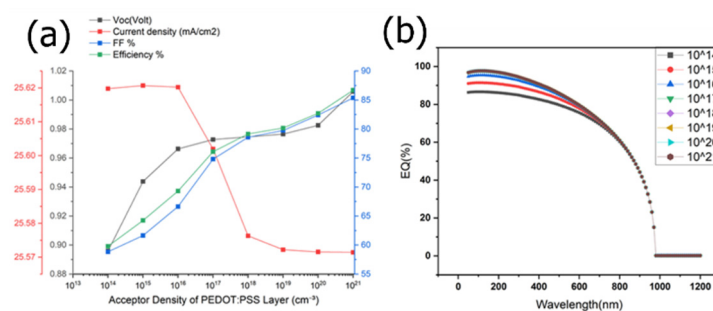


Figure 6. (a) The effect of acceptor density in the PEDOT: PSS layer on photovoltaic parameters (V_{OC} , J_{SC} , FF, and η), and (b) the EQE as a function of wavelength for varying acceptor densities in the PEDOT: PSS layer

3.6 Temperature dependence on device performance

Here, as shown in **Figure 7**, we examine the performance of the device as a function of temperature. From **Figure 7a**, as the temperature rises from 273K to 333K, the V_{OC} decreases steadily from 0.984V at 273K to 0.956V.

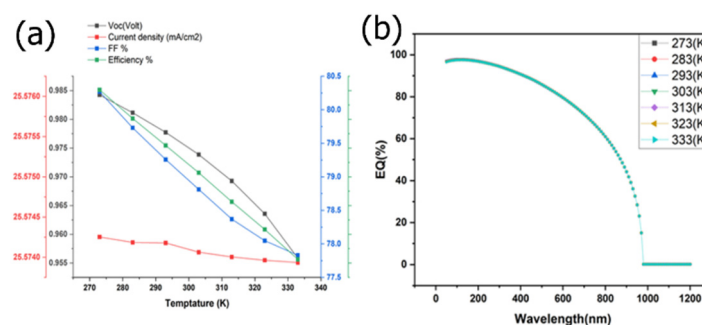


Figure 7. The effect of temperature on the (a) the changes in photovoltaic parameters (V_{OC} , J_{SC} , FF, and η) with varying temperatures, and (b) the EQE percentages

Similarly, the FF drops from 80.27% to 77.83%, and the overall efficiency of the device falls from 20.21% to 19.03%. The current density exhibits a notable degree of stability throughout the temperature range, suggesting that variations in V_{OC} , FF, and η are not attributable to substantial shifts in the current output. The lowest temperature, 273K, where the maximum values of V_{OC} , FF, and η are measured, is where best performance is observed. As can be seen from

the EQE spectrum in **Figure 7b**, the EQE of the device is largely constant between 273K and 333K. This stability indicates that the capacity of the device to convert photons into electrons over the reported wavelength range is mostly unaffected by temperature fluctuations. This stability in EQE, in contrast to other performance metrics like V_{OC} , FF, and η , suggests that the main photoactive processes are less susceptible to temperature variations than the device's total electrical performance.

4. OPTIMIZED DEVICE

The optimum parameters for our photodetector device are given in **Table 2**. The active layer thickness was set to 800 nm, the PEDOT: PSS HTL to 50 nm, and the PFN:Br ETL to 5 nm. The shallow uniform acceptor density (nA) of the active layer was optimized to $7.5 \times 10^{16} \times cm^{-3}$, while the shallow uniform donor density (nD) of PFN: Br (ETL) and the shallow uniform acceptor density (nA) of PEDOT: PSS (HTL) were both set to $10^{21} \times cm^{-3}$. Our device structure (FTO/PFN:Br/PBDB-T-2F:BTP-4F /PEDOT:PSS/Ag) differs significantly from the structure used in the work by N.I.M. Ibrahim et al. (ITO/PEDOT:PSS/PBDB-T-2F:BTP-4F/PFN/Ag)[33]. By changing the order of the HTL and ETL layers, we were able to achieve superior performance. Specifically, after optimizing layer thickness and doping concentrations.

Table 2. Optimized numerical parameters

Parameters	Value
Thickness of Active layer	800 nm
Thickness of PEDOT: PSS (HTL)	50 nm
Thickness of PFN:Br (ETL)	5 nm
Shallow uniform acceptor density, nA of Active layer	$7.5 \times 10^{16} cm^{-3}$
Shallow uniform donor density, nD of PFN:Br (ETL)	$1 \times 10^{21} cm^{-3}$
Shallow uniform acceptor density, nA of PEDOT: PSS (HTL)	$1 \times 10^{21} cm^{-3}$

The current density-voltage (J-V) characteristics of the photodetector device are displayed in **Figure 8a**, which also shows the dark current density and photocurrent density. A robust photoresponse is indicated by the photocurrent density (black line), which peaks at about 35 mA/cm² slightly below 1 V under illumination. At low voltages, the dark current density (red line) stays low and only begins to climb noticeably at 0.2 V. According to the dark current density statistics, it is modest (between 10^{-18} and 10^{-15} A/cm²) until 0.2 V, at which point it climbs exponentially to 9.18 A/cm² at 1 V. This behavior indicates low leakage current at low voltages, which enhances the stability and efficiency of the device.

The quantum efficiency (QE) and responsivity (R) at wavelengths ranging from 200 nm to 1200 nm are shown in **Figure 8b**. Between 300 and 900 nm, the QE (black line) stays high and nearly 100%, demonstrating the device's remarkable photon-to-electron conversion efficiency. In the same spectral region, the responsivity (red line) peaks at approximately 0.66 A/W, suggesting great sensitivity. Beyond 900 nm, photon energy decreases and QE and responsivity both decrease. According to comprehensive statistics, QE and responsivity peak at 800 nm and then steadily decline from 50 nm to 800 nm. Performance is at its best at 800 nm, where QE is 97.68% and responsivity is 0.63 A/W. These findings highlight the device's excellent sensitivity and efficiency overall, making it appropriate for applications requiring accurate light detection over a wide spectral range.

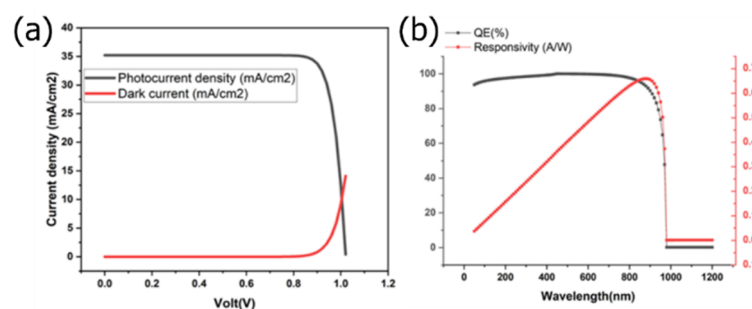


Figure 8. (a) J-V characteristic curve of the optimized photodetector, and (b) QE and responsivity as functions of wavelength.

Table 3. A comparative analysis of the performance of various OPDs from different studies, highlighting the advancements achieved in this work

Active Materials	V_{OC} (V)	J_{sc} (mA/cm ²)	FF (%)	PCE (%)	Ref.
Experimental Results					
PEDOT: PSS/GO/PCDTBT: PC71BM	0.82	10.44	50.0	4.28	[34]
PEDOT: PSS/GO/PCDTBT: PC71BM	0.85	10.82	57.0	5.24	[35]
PEDOT: PSS/PTB7:PC71BM	0.74	14.89	74.08	5.92	[36]
PTB4/PC71BM	0.70	14.80	64.60	7.1	[37]
PEDOT: PSS/PTB7-Th: PC61BM	0.78	17.66	52.41	7.24	[38]

Active Materials	Voc (V)	Jsc (mA/cm ²)	FF (%)	PCE (%)	Ref.
PEDOT: PSS/PBDB-T: ITIC-OE	0.96	16.50	69.75	11.0	[39]
PEDOT: PSS/PBDB-T: ITIC	1.06	16.20	82.95	14.25	[40]
CuI/PBDB-T: ITIC	0.98	20.15	79.59	15.68	[41]
PBD: PFBSA/PBDB-T: N2200	0.85	24.23	71.0	16.2	[42]
Simulation Results					
GO/PBDB-T: ITIC	0.9148	25.71	58.45	13.74	[32]
GO/PTB7:PC71BM	0.9070	18.12	61.30	10.07	[32]
PEDOT: PSS/PBDB-T-2F: BTP-4F/PFN-Br	0.25	29.14	56.44.4	4.1	[33]
PFN-Br /PBDB-T-2F: BTP-4F/ PEDOT: PSS	1.02	35.20	84.61	30.40	This work

CONCLUSIONS

This study highlights the notable enhancements in photodetector performance that may be obtained by carefully adjusting layer thicknesses and doping densities with the use of SCAPS-1D simulations. Through structural modification, we were able to create a significantly higher efficiency device configuration than that suggested by N. I. M. Ibrahim et al. using modifications in the HTL and ETL layers, the optimized structure using FTO/PFN/PBDB-T-2F/PEDOT/Ag shown notable improvements in V_{OC} , J_{SC} , FF, and overall efficiency. Furthermore, the device displayed a high EQ exceeding 99% and responsivity reaching up to 0.65 A/W throughout a broad spectral area from 300 nm to 900 nm. These results pave the way for more effective devices in real-world applications by highlighting the significance of layer arrangement and material qualities in generating high-performance photodetectors.

Acknowledgments

The authors would like to acknowledge that this paper has been submitted in part. fulfillment of the requirements for a PhD degree at Yildiz Technical University.

Funding Declaration: This research received no specific grant from any funding agency in the public, commercial, or not-for-profit sectors.

Competing Interest Declaration: The authors declare that there are no competing interests.

ORCID

✉ **Ahmet Sait Alali**, <https://orcid.org/0000-0002-7750-5571>; ✉ **Murat Oduncuoglu**, <https://orcid.org/0000-0002-3130-5646>

✉ **Hmoud Al-Dmour**, <https://orcid.org/0000-0001-5680-5703>

REFERENCES

- [1] G. Luo, *et al.*, "Boosting the Performance of Organic Photodetectors with a Solution-Processed Integration Circuit toward Ubiquitous Health Monitoring," *Advanced Materials*, **35**(36), 2301020 (2023). <https://doi.org/10.1002/adma.202301020>
- [2] N.S. Hamzah, and E.K. Hassan, "Fabrication and Enhancement of Organic Photodetectors Based on Iron Phthalocyanine Films, *International Journal of Nanoscience*, (2024). <https://doi.org/10.1142/S0219581X2350028X>
- [3] J.-W. Qiao, F.-Z. Cui, L. Feng, P. Lu, H. Yin, and X.-T. Hao, "Efficient Ultrathin Self-Powered Organic Photodetector with Reduced Exciton Binding Energy and Auxiliary Förster Resonance Energy Transfer Processes," *Advanced Functional Materials*, **33**(30), 2301433 (2023). <https://doi.org/10.1002/adfm.202301433>
- [4] W. Liu, Q. Liu, J. Xiao, Y. Wang, L. Yuan, H. Tai, and Y. Jiang, "Performance enhancement of an organic photodetector enabled by NPB modified hole transport layer," *IOPscience*, **55**, 234001 (2024). <https://doi.org/10.1088/1361-6463/ac5990>
- [5] P. Jacoutot, *et al.*, "Enhanced sub-1 eV detection in organic photodetectors through tuning polymer energetics and microstructure," *Science Advances*, **9**(23), eadh2694 (2023). <https://doi.org/10.1126/sciadv.adh2694>
- [6] X. Yan, X. Wang, S. Gao, and W. Qiao, "High-Performance Organic Photodetectors Using SnO₂ as Interfacial Layer with Optimal Thickness," *Physica Status Solidi (a)*, **220**(1), 2200667 (2023). <https://doi.org/10.1002/pssa.202200667>
- [7] P. Corral, F. Rodriguez-Mas, G.D. Scals, D. Valiente, J.C. Ferrer, and S.F. de Avila, "Improvements of Organic Photodetectors for VLC Using a New Active Layer, Focal Lens, and a Transimpedance Amplifier," *Elektronika ir Elektrotechnika*, **28**(4), 4 (2022). <https://doi.org/10.5755/j02.eie.31292>
- [8] J. Kang, *et al.*, "Enhanced Static and Dynamic Properties of Highly Miscible Fullerene-Free Green-Selective Organic Photodetectors," *ACS Appl. Mater. Interfaces*, **13**(21), 25164–25174 (2021). <https://doi.org/10.1021/acsami.1c02357>
- [9] J. Wang, *et al.*, "Enhanced photomultiplication of organic photodetectors via phosphorescent material incorporation," *J. Mater. Chem. C*, **9**(47), 16918–16924 (2021). <https://doi.org/10.1039/D1TC04524E>
- [10] G. Manzoor, K.K. Sharma, G.K. Bharti, and D. Nath, "Modelling and Performance Analysis of CuPc and C60 Based Bilayer Organic Photodetector," *IJEER*, **10**(4), 811–816 (2022). <https://doi.org/10.37391/ijeer.100408>
- [11] W. Teng, W. Yanbin, J. Chen, and B. Wang, *Active layer used for ternary blending solar cell and application of active layer*, (2018). [Online Video]. <https://typeset.io/papers/active-layer-used-for-ternary-blending-solar-cell-and-2rxfqsn5q>
- [12] B.-K. Choo, S. Ahn, B.-Ho Cheong, J.-w. Cho, H.-J. Cho, and H.S. Yeon, Active layer of thin film transistor crystallizing apparatus and the crystallizing method using the same, (2015). [Online Video]. <https://typeset.io/papers/active-layer-of-thin-film-transistor-crystallizing-apparatus-j6u2d4hdjw>
- [13] J. Tard, J. Pauchet, R. Vincent, Formulation of an active layer having improved performances, (2013). [Online Video]. <https://typeset.io/papers/formulation-of-an-active-layer-having-improved-performances-39t79hc0se>

- [14] Y. Zheng, Y. Cheng, L. Li, Active bio piezoelectric ceramic coating layer and method of preparing said coating layer on titanium base body surface, (2006). [Online Video]. <https://typeset.io/papers/active-bio-piezoelectric-ceramic-coating-layer-and-method-of-30leypt5z1>
- [15] R.-K. Shiu, *et al.*, “Performance Enhancement of Optical Comb Based Microwave Photonic Filter by Machine Learning Technique,” *Journal of Lightwave Technology*, **38**(19), 5302–5310 (2020). <https://doi.org/10.1109/JLT.2020.2989210>
- [16] Y. Wang, *et al.*, “Organic photovoltaics with 300 nm thick ternary active layers exhibiting 15.6% efficiency,” *J. Mater. Chem. C*, **9**(31), 9892–9898 (2021). <https://doi.org/10.1039/D1TC02748D>
- [17] L. Zhan, *et al.*, “Layer-by-Layer Processed Ternary Organic Photovoltaics with Efficiency over 18%,” *Advanced Materials*, **33**(12), 2007231 (2021). <https://doi.org/10.1002/adma.202007231>
- [18] J. Gao, *et al.*, “Over 16.7% efficiency of ternary organic photovoltaics by employing extra PC71BM as morphology regulator,” *Sci. China Chem.* **63**(1), 83–91 (2020). <https://doi.org/10.1007/s11426-019-9634-5>
- [19] T. Kong, *et al.*, “A Newly Crosslinked-double Network PEDOT:PSS@PEGDMA toward Highly-Efficient and Stable Tin-Lead Perovskite Solar Cells,” *Small*, **19**(40), 2303159 (2023). <https://doi.org/10.1002/sml.202303159>
- [20] L. Jin, J. W. Zhang, and S. Ju, “Preparation and Properties of PEDOT:PSS-Based Thermoelectric Thin Films,” *Materials Science Forum*, **1070**, 173–181 (2022). <https://doi.org/10.4028/p-pmw1c6>
- [21] Y. Zhou, *et al.*, “Effects of PEDOT:PSS:GO composite hole transport layer on the luminescence of perovskite light-emitting diodes,” *RSC Adv.* **10**(44), 26381–26387 (2020.). <https://doi.org/10.1039/D0RA04425C>
- [22] L. Liu, H. Yang, Z. Zhang, Y. Wang, J. Piao, Y. Dai, and B. Cai, “Photopatternable and Highly Conductive PEDOT:PSS Electrodes for Flexible Perovskite Light-Emitting Diodes,” *ACS Appl. Mater. Interfaces*, **15**(17), 21344–21353 (2023). <https://doi.org/10.1021/acsami.3c03108>
- [23] H. Fu, *et al.*, “High-performance Ag nanowires/PEDOT:PSS composite electrodes for PVDF-HFP piezoelectric nanogenerators,” *J. Mater. Sci: Mater. Electron.* **32**(16), 21178–21187 (2021). <https://doi.org/10.1007/s10854-021-06616-9>
- [24] A. Pisciotta, *et al.*, “PEDOT: PSS promotes neurogenic commitment of neural crest-derived stem cells,” *Front. Physiol.* **13**, (2022). <https://doi.org/10.3389/fphys.2022.930804>
- [25] S.A. Moiz, M.S. Alzahrani, and A.N.M. Alahmadi, “Electron Transport Layer Optimization for Efficient PTB7:PC70BM Bulk-Heterojunction Solar Cells,” *Polymers*, **14**(17), 3610 (2022). <https://doi.org/10.3390/polym14173610>
- [26] A. Ait Abdelkadir, and M. Sahal, “Theoretical development of the CZTS thin-film solar cell by SCAPS-1D software based on experimental work,” *Materials Science and Engineering: B*, **296**, 116710 (2023). <https://doi.org/10.1016/j.mseb.2023.116710>
- [27] S. Chowdhury, A.S. Najm, M. Luengchavanon, A.M. Holi, C.H. Chia, K. Techato, and S. Channumsin, “Investigating the Effect of Nonideal Conditions on the Performance of a Planar Sb₂Se₃-Based Solar Cell through SCAPS-1D Simulation,” *Energy & Fuels*, **37**(9), 6722–6732 (2024). <https://doi.org/10.1021/acs.energyfuels.2c03593>
- [28] M. Abdelfatah, A.M. El Sayed, W. Ismail, S. Ulrich, V. Sittinger, and A. El-Shaer, “SCAPS simulation of novel inorganic ZrS₂/CuO heterojunction solar cells” *Scientific Reports*, **13**, 4553 (2024). <https://www.nature.com/articles/s41598-023-31553-4>
- [29] Y. Hairch, Aelmelouky, M. Monkade, and R. Elmoznine, “Investigation of optical and electrical properties of CIGS solar cell using simulation program SCAPS and Impedance spectroscopy,” (2023). <https://doi.org/10.22541/au.167872056.62172198/v1>
- [30] Sk.T. Ahamed, A. Basak, and A. Mondal, “Device modeling and investigation of Sb-based low-cost heterojunction solar cells using SCAPS-1D,” *Results in Optics*, **10**, 100364 (2023). <https://doi.org/10.1016/j.rio.2023.100364>
- [31] M. Muzammil, K.N. Naam, M. Fareed, M.S. Hussain, and M. Zulfiqar, “Boosting the performance of PBDB-T/ITIC based organic solar cell: A theoretical analysis utilizing SCAPS-1D,” *Chemical Physics Impact*, **8**, 100407 (2024). <https://doi.org/10.1016/j.chphi.2023.100407>
- [32] G.A. Nowsherwan, *et al.*, “Performance Analysis and Optimization of a PBDB-T:ITIC Based Organic Solar Cell Using Graphene Oxide as the Hole Transport Layer,” *Nanomaterials*, **12**(10), (2022.). <https://doi.org/10.3390/nano12101767>
- [33] N.I.M. Ibrahim, A.M. Elharbi, and A. Albadri, “Study the Effect of Thickness on the Performance of PM6:Y6 Organic Solar Using SCAPS Simulation,” *AMPC*, **14**(04), 55–65 (2024). <https://doi.org/10.4236/ampc.2024.144005>
- [34] S. Rafique, S.M. Abdullah, M.M. Shahid, M.O. Ansari, and K. Sulaiman, “Significantly improved photovoltaic performance in polymer bulk heterojunction solar cells with graphene oxide /PEDOT:PSS double decked hole transport layer,” *Sci Rep*, **7**(1), 39555 (2017). <https://doi.org/10.1038/srep39555>
- [35] S. Rafique, *et al.*, “UV- ozone treated graphene oxide/ PEDOT:PSS bilayer as a novel hole transport layer in highly efficient and stable organic solar cells,” *Organic Electronics*, **66**, 32–42 (2019). <https://doi.org/10.1016/j.orgel.2018.12.005>
- [36] K. Tan, P. Lin, G. Wang, Y. Liu, Z. Xu, and Y. Lin, “Controllable design of solid-state perovskite solar cells by SCAPS device simulation,” *Solid-State Electronics*, **126**, 75–80 (2016). <https://doi.org/10.1016/j.sse.2016.09.012>
- [37] L. Lu, and L. Yu, “Understanding Low Bandgap Polymer PTB7 and Optimizing Polymer Solar Cells Based on It,” *Advanced Materials*, **26**(26), 4413–4430 (2014). <https://doi.org/10.1002/adma.201400384>
- [38] H. Lian, J. Ning, A. Bolag, A. Hexig, N. Gerile, O. Tegus, and S. Lin, “Optimization of PEDOT:PSS Hole Transport Layer Toward the Organic Solar Cells with High Fill Factor,” *Scientific. Net.* 113-118 (2024). <https://www.scientific.net/SSP.288.113>
- [39] K.S. Nithya, and K.S. Sudheer, “Numerical modelling of non-fullerene organic solar cell with high dielectric constant ITIC-OE acceptor,” *J. Phys. Commun.* **4**(2), 025012 (2020). <https://doi.org/10.1088/2399-6528/ab772a>
- [40] W. Abdelaziz, A. Shaker, M. Abouelatta, and A. Zekry, “Possible efficiency boosting of non-fullerene acceptor solar cell using device simulation,” *Optical Materials*, **91**, 239–245 (2019). <https://doi.org/10.1016/j.optmat.2019.03.023>
- [41] K.S. Nithya, and K.S. Sudheer, “Device modelling of non-fullerene organic solar cell with inorganic CuI hole transport layer using SCAPS 1-D,” *Optik*, **217**, 164790 (2020). <https://doi.org/10.1016/j.ijleo.2020.164790>
- [42] T.N.L. Phan, J. Kim, G.-U. Kim, S. Lee, and B.J. Kim, “Aniline-based hole transporting materials for high-performance organic solar cells with enhanced ambient stability,” *Journal of Materials Chemistry A*, (RSC Publishing). (2024). <https://pubs.rsc.org/en/content/articlelanding/2021/xx/d1ta03665c/unauth>

**ОПТИМІЗАЦІЯ ОРГАНІЧНИХ ФОТОДЕТЕКТОРІВ ЗА ДОПОМОГОЮ МОДЕЛЮВАННЯ SCAPS-1D:
ПІДВИЩЕННЯ ПРОДУКТИВНОСТІ ПРИСТРОЇВ НА ОСНОВІ PBDB-T-2F ШЛЯХОМ КОНФІГУРАЦІЇ ШАРУ
ТА РЕГУЛЮВАННЯ ЛЕГУВАННЯ**

Ахмет Саїт Алалі^а, Мурат Одункуоглу^а, Хмуд Аль-Дмур^б, Абделааль С.А. Ахмед^с

^а*Факультет фізики, Технічний університет Йилдиз, Стамбул, Туреччина*

^б*Університет Мута, факультет природничих наук, кафедра фізики, 61710, Йорданія*

^с*Кафедра хімії, Факультет природничих наук, Університет Аль-Азхар, Ассуїт, 71524, Єгипет*

У цьому дослідженні ми провели дослідження оптимізації різних параметрів фотодетектора за допомогою моделювання SCAPS-1D для підвищення його загальної продуктивності. Конструкцію фотоприймача модифіковано на основі структури, запропонованої Н.І.М. Ібрагім та ін. (AMPC, 14(04), 55–65 (2024) шляхом зміни порядку шару транспортування дірок (HTL) та шару транспортування електронів (ETL). Завдяки оптимізації товщини шару та концентрації легування ми значно покращили фотоелектричні параметри нашої оптимізованої структури (FTO/PFN/PBDB-T-2F/PEDOT/Ag). 1,02 В, JSC 35,20 мА/см², FF 84,61 % і загальний ККД 30,40 % Крім того, пристрій продемонстрував високу квантову ефективність (EQ) понад 99 % і чутливість із піком 0,65 А/Вт, охоплюючи широка спектральна область від 300 нм до 900 нм результати вказують на критичну роль ретельної оптимізації при розробці високоефективних фотодетекторів, надаючи цінну інформацію про проектування та виготовлення пристроїв із чудовими характеристиками продуктивності.

Ключові слова: *органічний фотодетектор; моделювання SCAPS-1D; оптимізація продуктивності; PBDB-T-2F; BTP-4F; PEDOT; PSS; PFN; Br*